Cyclic Behavior of High-Strength Steel Beam-to-Column Welded Flange-Bolted Web Connections

Fangxin Hu[a,b,*], Zhan Wang[a,b]

[a] *School of Civil Engineering and Transportation, South China University of Technology, Guangzhou, 510640, China*
[b] *State Key Laboratory of Subtropical Building and Urban Science, South China University of Technology, Guangzhou, 510640, China*

Abstract

Four Q690 high-strength steel beam-to-column moment connections, which use welded joints between beam and column flanges as well as a bolted beam web to the column flange, were tested under cyclic loading. The effects of beam-to-column welding details and panel zone strength were studied. Two pairs of welded flange details were incorporated, including the Chinese code-specified complete-joint-penetration (CJP) welded connections with backing plates where the bottom backing plate is reinforced by a fillet weld, and enhanced CJP welded connections with backing plates removed, weld roots backgouged, and further reinforced by fillet welds. Three panel zone thicknesses were designed to characterize strong, intermediate and weak panel zones, respectively. The test results show that backing plates should be removed in these moment connections to prevent brittle weld fracture, but still rendering only limited plastic hinge rotations in the order of 0.01–0.02 rad in the beam end before ductile fracture of the beam flange. The panel zone, however, survived even after a plastic shear rotation of 0.03 rad, demonstrating much higher plastic deformation capacity than the beam plastic hinge. This suggests that ductility can be exploited in 690 MPa high-strength steel panel zones, but not reliably in 690 MPa steel beams.

Keywords: High-strength steel, Beam-to-column connection, Moment connection, Welded flange-bolted web connection, Cyclic, Experiment

*Corresponding author
Email address: `hufx@scut.edu.cn` (Fangxin Hu)

1 Introduction

High-strength steels with a nominal yield strength no less than 460 MPa have a great deal of benefits over conventional-strength steels. By using high-strength steels, the increased cross-sectional strength results in reduced structural weight for the same loading condition [1–6], and thereby allows for more economical and ecological construction. The increased elastic deformation capacity of high-strength steels makes them suitable for structural members to remain elastic under strong earthquakes, which means these steels have a great potential to be used in seismic resilient steel structures, such as in self-centering structures [7–9]. In spite of their much higher yield and ultimate tensile strength, high-strength steels have much lower ductility, in terms of the fracture strain or elongation, than conventional steels [10–12]. This greatly impacts the inelastic behavior of structural members or connections. It is well known that ductility of moment-resisting connections is important for satisfactory seismic performance of steel moment frames, but these moment connections made of high-strength steels have not been scrutinized. Regarding inelastic behavior under monotonic or cyclic loading, a limited number of studies have been conducted on high-strength steel welded flange-welded web connections [13–16], welded flange-bolted web connections [17–21], bolted extended/flush end-plate connections [14, 22–33], cover-plate/flange-plate/stiffener/haunch reinforced connections [15, 16, 18, 19, 34–41] as well as column web panels subjected to shear [42–44]. Among the above various connection types, beam-to-column welded-flange connections, including welded flange-welded web and welded flange-bolted web connections, are still the most popular connections in steel construction, both owing to their fully restrained property and convenient fabrication as well as erection in practice.

Kuwamura and Suzuki [13] tested seven beam-to-column connections subjected to cyclic loading of different constant displacement amplitudes. These connection specimens were made of 600MPa tensile-strength grade high-strength steel with yield ratios less than 80%. The beam-to-column flanges were grooved and complete-joint-penetration (CJP) welds were used with flux backing plates. It should be noted that these backing plates were removed after welding and reinforcing fillet welds were applied. No scallops or weld access holes were needed as these groove welds were completed in the fabrication shop using a flux-core arc welding (FCAW) process. Two levels of heat input (20 kJ/cm and 60 kJ/cm) were examined. The results show that these connections with a small-size beam (H-shaped section of H200×100×9×9 mm) sustained substantial cumulative plastic deformation. Kuwamura and Suzuki [13] also concluded that the connections had an enough safety margin against the prescribed strong earthquake motion in Japan by comparing the average and cumulative ductilities revealed in the tests with the demands from seismic analysis.

Dubina et al. [14] evaluated eight types of beam-to-column moment connections through both monotonic- and cyclic-loading tests, among which one type was the fully welded connection constructed from a mild steel (S235) beam and high-strength steel (S460) column, strengthened by vertical stiffeners outside the beam flanges. The beam and column flanges were connected using CJP groove welds without access holes or backing plates, while the beam web was fillet welded to the column. Metal active-gas welding (MAG) was used. After buckling of the stiffener and beam flange under compression, and some shear deformation of the panel zone, this specimen finally failed by weld crack initiation at the stiffener in tension. It developed large rotation exceeding 0.06 rad under cyclic loading, and nearly 0.1 rad under monotonic loading. These rotation capacities were all contributed by the panel zone.

Oh and Park [15] assessed eight beam-to-column connections made of HSA800 grade steel (tensile strength above 800 MPa and yield strength between 650 and 770 MPa) under cyclic loading, among which one connection had traditional weld details (CJP groove welds at the beam flanges with backing plates and weld access holes, and two-side fillet welds at the beam web), and another connection used the non-scallop (no-access-hole) welding method that removed backing plates and reinforced the CJP weld root with fillet welds. They observed that the traditional welded connection developed very limited plastic rotation less than 0.01 rad, while the non-scallop connection sustained nearly 0.02 rad.

Liao et al. [16] tested four beam-to-column cruciform welded flange-welded web connections made of Q460D (460 MPa) steel in China under cyclic loading. One of the connections used the traditional weld details and weld access hole geometry specified in Chinese Technical Specification [45], where backing plates were used for CJP groove welds at both beam flanges but only the backing plate below the bottom beam flange was reinforced by a fillet weld beneath. Another two of the connections used the suggested improved access hole geometries in Chinese Technical Specification [45] and FEMA-350 [46], respectively, while their weld details were the same to the previous. It was reported that these connections sustained ultimate displacements of 80–90 mm, or story drift angles of 0.053–0.06 rad, demonstrating substantial deformation capacity. No significant effect of the weld access hole geometry in these connections was found.

Nie et al. [19] tested four beam-to-column one-sided moment connections made of Q690GJNHE (690 MPa) steel in China under cyclic loading, among which two were welded flange-bolted web connections and differed in cross-sectional slenderness of the beam and column. The beam flanges were CJP groove welded to the column using ceramic backing plates which could be easily removed after welding. The improved weld access hole details in Chinese Technical Specification [45] were followed and rich argon gas-shielded metal arc welding (GMAW) process was used. The beam web was connected to the column through a pair of shear tabs by four high-strength bolts. The two specimens experienced fracture in heat-affected zone (HAZ) of the beam groove weld, and developed plastic deformation of about 20 mm, corresponding to a plastic rotation of about 0.012 rad. The specimen with more slender beam and column sections was found to sustain slightly lower plastic deformation that the other one.

Qiang et al. [20] evaluated four beam-to-column welded flange-bolted web connections through monotonic-loading tests under ambient and elevated temperatures. Two specimens, made of Q690 and Q960 high-strength steels in China, respectively, were tested monotonically under an ambient temperature. It seems that the beam flanges were connected to the column using CJP groove welds without any backing plate, but the details on weld access holes were not provided. Interestingly, the Q690 specimen failed by fracture between the column flange and the column web and continuity plate, while the Q960 specimen underwent fracture in the beam flange-to-column groove weld. The column flange-to-continuity plate fracture in the previous specimen seemed to be caused by the misuse of fillet welds, whereas current codes generally also require CJP groove welds for continuity plates. Nevertheless, the Q690 specimen developed large connection rotation of almost 0.06 rad, while the Q960 specimen developed only a half.

Liu et al. [17] tested four Q460C (460 MPa) steel beam-to-column welded flange-bolted web connections subjected to cyclic loading. These connections had different welding details. Two weld access hole shapes (the standard shape in Chinese Seismic Code [47] and improved shape in FEMA-350 [46]) were examined, as well as four details related to backing plates (i.e., steel backing plates left in place, backing plates removed and weld roots backgauged and fillet-reinforced, backing plates reinforced by fillet welds beneath, ceramic backing plate removed after welding). All specimens underwent crack initiation at the termination of beam flange groove weld and finally fracture through the beam flange. They developed considerable plastic rotations of 0.02–0.03 rad. As expected, the connection using ceramic backing plates sustained the largest cumulative plastic deformation, followed by the connection with backing plates removed after welding. The other two connections with backing plates, reinforced by fillet welds or not, behaved very similarly.

Lu [18] tested eight (four one-sided and four cruciform) moment connections under cyclic loading, among which the connections made of Q460GJ (460 MPa), Q550GJ (550 MPa) and Q690GJ (690 MPa) steels, respectively, had the typical welded flange-bolted web detailing. For the CJP groove welds between the beam and column flanges, backing plates were used and left in place. No fillet welds were added for reinforcement. These specimens had a strong panel zone so that the plastic hinge was expected in the beam end. Except for the Q460GJ specimen, which developed a plastic rotation of about 0.012 rad, the Q550GJ and Q690GJ specimens hardly developed any plastic deformation since they fractured upon loading into the first significant post-yielding cycle.

The panel zone plays an important role in the seismic behavior of beam-to-column moment connections. Previous research have evidenced that moderate yielding in the panel zone may promote the total plastic rotation capacity, but too much shear distortion of the panel zone may be detrimental [41, 48]. Then it deserves to be examined how much shear distortion could be sustained by high-strength steel panel zones. Girão Coelho et al. [42] indicated through monotonic-loading tests that S690 and S960 shear panels could sustain shear distortions exceeding 0.05 rad, even above 0.1 rad, and this deformation capacity highly depended on the panel slenderness, aspect ratio and axial load level. Jordão et al. [43] also confirmed this superior inelastic performance. Further, Luo et al. [44] evaluated eight beam-to-column connections under cyclic loading, among which two connections had H-shape beams connected to H-shape columns using welded flange-welded web details. The CJP groove welds at the beam flanges used backing plates but weld access holes were not used. The connections developed plastic distortions of 0.025–0.035 rad in the panel zone before final fracture in the CJP welds. The real deformation capacity of this steel panel zone should be somewhat higher since the panel zones in the specimens remained intact. Interestingly, the premature fracture of the CJP weld, which used a matching weld filler material, occurred but the beam in the above specimens developed little plastic deformation.

Recently, the authors [21] tested five welded flange-bolted web connections, in which beams and columns were made of Q355 (355 MPa) conventional steel and Q690 high-strength steel, respectively. The authors discovered that for both traditional [45] and improved [46] weld access holes, the CJP groove weld connecting the Q355 beam flange to the Q690 column with a backing plate, where the weld metal matched with the beam steel grade, could develop substantial plastic rotation reaching 0.03 rad. This rotation even qualifies for special moment frames in AISC Seismic

Provisions [49], which may partly be attributed to the relatively shallow beam (320 mm in depth) used in the tests compared to the United States practice. More interestingly, it was found that the Q690 panel zone experienced a plastic rotation of 0.04 rad before its shear fracture. This data provides the reference rotation capacity of the panel zone made of 690 MPa high-strength steel.

In spite of the previous studies, limited evidence is available in China for high-strength steel welded flange-welded/bolted web moment connections, especially those connections using 690 MPa or higher grade steel. Note that, several tests have indicated quite limited rotation capacity of 690 MPa steel beam plastic hinge formed at the column face [15, 18, 19, 44], while the 690 MPa steel panel zone seems to behave in a very ductile manner [21, 44]. Therefore, to provide further evidence, an experimental program was conducted to develop confidence and fundamental data related to the rotation capacity of welded unreinforced flange-bolted (WUF-B) web moment connections made of Q690 steel in China. Four specimens were tested under cyclic loading to examine their seismic performance in this paper, to supplement previous tests on dual-steel moment connections [21]. The plastic rotation and energy dissipation capacities revealed by this study are aimed at developing design guidelines for this connection and evaluating seismic performance of corresponding moment frames.

2 Test program

2.1 Design of specimens

This paper focuses on investigating the T-shaped subassemblage, which represents a connection between an exterior column and beam in a moment frame structure. The dimensions of the beam and column in the subassemblage were determined based on an appropriate design of a three-bay six-story plane moment frame prototype, as illustrated in Figure 1. The applied dead (D) and live (L) loads are 6 kN/m^2 and 2 kN/m^2, respectively. The height of each story (H) is 3000 mm, and both the in-plane and out-of-plane column spacing (L) are 6000 mm. Under lateral loads like earthquakes, it is anticipated that the prototype frame will experience reverse curvature bending in both the columns and beams, with inflection points occurring near the mid-span of the beams and the mid-height of the columns. This assumption holds true when the seismic load is significantly larger than the gravity load. In the T-shaped specimen, load pins were employed at the top and bottom of the column to simulate the column inflection points, while the beam inflection point was simulated by the free end of the beam where the actuator is attached. Further details can be found in the subsequent section.

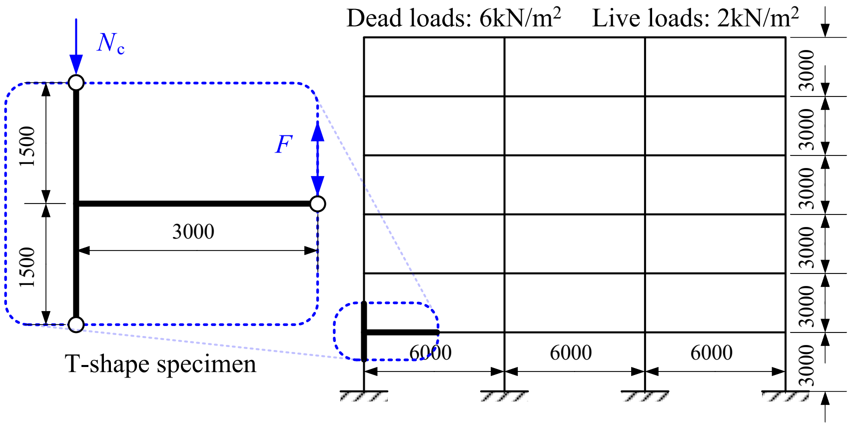

Figure 1. Extraction of the T-shaped assembly (unit: mm)

Both beams and columns in the prototype frame were fabricated using high-strength (grade Q690) steel in China. Both ultimate and serviceability limit states were considered for these members. Regarding the ultimate limit state, beam strength, column strength, and stability were assessed using a factored non-seismic load combination of 1.3D + 1.5L. Additionally, strength and stability requirements were met under a different factored seismic load combination of 1.2 (D + 0.5L) + 1.3E_{hk1}, where E_{hk1} represents the design seismic action of the minor earthquake (1st-group, intensity-8 and ground type II), as per the regulations outlined in Chinese Seismic Code [47]. Typically, it is essential to provide sufficient bracing for beams in earthquake-resistant frames to prevent lateral-torsional buckling. Therefore, beam instability was not considered in this analysis. For the serviceability limit state, the maximum beam deflection was checked against the code-specified limit of 1/400 of the beam span under a nominal non-seismic load combination of D + L. Furthermore, the maximum story drift angle imposed by the minor earthquake mentioned earlier was required to remain below 1/250. Consequently, a built-up H-shaped section with dimensions of H280×160×8×10 was selected for the beams, while two design outcomes with built-up H-shaped sections, namely H220×160×12×16 and H220×160×16×16, for the columns were achieved. Further, another design was implemented to reinforce the column section H220×160×12×16 with a 8-mm-thick doubler plate in beam-to-column connections, indicating a total thickness of 20 mm for the panel zone. These sections differ only in terms of the panel zone thickness (including the doubler plate, if appropriate) but all satisfy strong column-weak beam (SCWB) capacity design, thereby enabling the evaluation of the panel zone strength impact.

Four specimens were designed for the purpose of this study. The design details are summarized in Table 1. The connection specimens were constructed with CJP groove welds, which efficiently connect the beam flanges to the column flange. Additionally, an erection plate (or shear tab) of the same steel grade and thickness as the beam web was shop-welded to the column flange using fillet welds, and bolted to the beam web to transfer shear force. In each specimen, three class 10.9s M20 high-strength bolts were utilized, with a pretension force of 155 kN [50], for the web connection. To ensure structural integrity, continuity plates of matching steel grade, width, and thickness to the beam flanges were incorporated in the investigation. These continuity plates serve two purposes: protecting the column flange and web from local damage and ensuring uniform stress distribution in the beam flanges. In addition to the varying panel zone thickness, two types of CJP groove weld details between the beam and column flanges, as depicted in Figure 2, were analyzed for comparison. The first type, labeled as "*b*" (Figure 2(a)), represents the current requirement in China (i.e., suggested in both Chinese Seismic Code [47] and Technical Specification [45]) and commonly employed in practice. In this type, a reinforcing fillet weld is applied under the bottom backing plate, while the top backing plate remains unreinforced. The weld access hole is machined according to the improved shape proposed in FEMA-350 [46] and further suggested in AISC Prequalified Connections [51]. This hole shape has been shown to alleviate stress concentrations in the transition region between the beam flange and the drilled hole. The second type, labeled as "*c*" (Figure 2(b)), is a suggested welded-flange connection detail in AISC Prequalified Connections [51] after comprehensive investigations by SAC Joint Venture in the United States. The backing plates underneath both beam flanges are removed, and the weld root is backgouged and further reinforced by a fillet weld. In spite of its relatively expensive process compared to Type *b*, this connection detail can largely improve its deformation performance and the connection rotation capacity can be enhanced substantially. Consequently, the specimen labels shown in Table 1 comprise the beam and column steel grades, followed by the panel zone thickness, and conclude with either *b* or *c* indicating the beam-to-column flange welded connection detail.

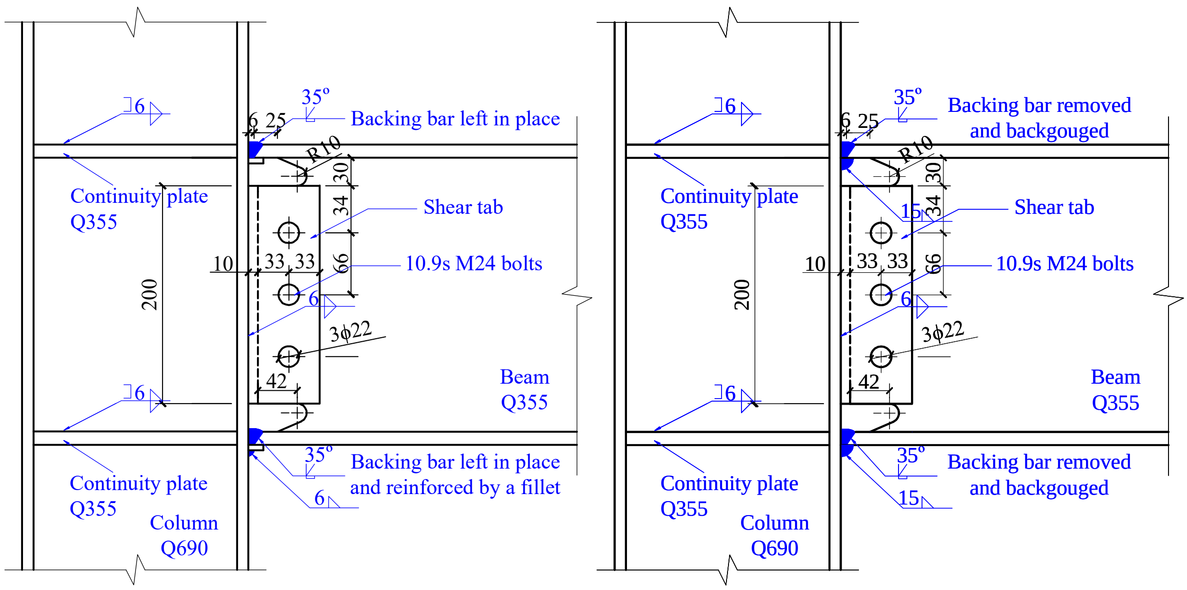

(a) Type *b*　　(b) Type *c*

Figure 2. Connection details

The research employed manual gas-shielded metal arc welding (GMAW) process in fabrication by use of matched weld filler materials with Q690 high-strength steel in China. An E761T1-K3C electrode was utilized, as specified in the recently published Chinese Design Standard for High-

Table 1. Test specimens

Specimen label	Beam section (mm)	Column section (mm)	Doubler plate (mm)	Welding type
B690-C690-PZ12*c*	H280×160×8×10	H220×160×12×16	None	*c*
B690-C690-PZ16*b*		H220×160×16×16	None	*b*
B690-C690-PZ16*c*		H220×160×16×16	None	*c*
B690-C690-PZ20*c*		H220×160×12×16	8	*c*

Strength Steel Structures (JGJ/T 483) [52], for all the welding work, including the fillet welds in the welded H-shaped beam and column sections, the CJP groove welds and the fillet welds for reinforcement, the fillet welds attaching the shear tab to the column flange, as well as the welds between continuity plates and the column. This electrode has proof (yield) and ultimate strength of 701 and 800 MPa, respectively, and its average Charpy v-notch toughness is about 57 J under a temperature of −20°C, according to the mill report.

2.2 Material properties

All steel plates utilized in the experiment, which have also been used in a previous study on dual-steel moment connections by the authors [21], underwent tensile coupon testing to analyze their stress-strain behavior. These test results were then compared to the requirements outlined in the relevant codes governing high-strength steel plates. This validation process ensured the qualification of the steel plates used in this study. For each plate thickness, three coupons were subjected to testing. The coupons employed were of full thickness, possessing a gauge length of 50mm and a width of 20mm at the reduced portion. Several parameters were determined for each plate thickness, including the modulus of elasticity (E), the yield or proof strength (f_y), the strain at the end of the yield plateau (or at the initiation of the strain hardening phase of the stress-strain curve, ϵ_{st}) if applicable, the ultimate strength (f_u), the corresponding ultimate strain (ϵ_u), the yield-to-tensile strength ratio (f_y/f_u), and the percentage elongation after fracture based on the specified parallel length (δ) [53]. These values, which represent the averages of three coupons, are summarized in Table 2. Figure 3 illustrates the full-range engineering stress-strain curves of the Q690 grade steel coupons, which have been reported in the previous study by the authors [21]. Additionally, simple tensile testing was conducted on the class 10.9s M20 high-strength bolts utilized in the study, providing information regarding the modulus of elasticity (E), ultimate strength (f_u), and ultimate strain (ϵ_u). These results can also be found in Table 2.

Table 2. Material properties

Steel grade	Plate thickness (mm)	E (GPa)	f_y (MPa)	ϵ_{st}	f_u (MPa)	ϵ_u	f_y/f_u	δ
Q690	8	208.3	723	—	822	0.100	0.88	20%
	10	189.4	794	—	902	0.106	0.88	21%
	12	205.8	775	0.018	816	0.060	0.95	16%
	16	219.8	811	0.022	840	0.055	0.97	17%
10.9s	M20	206.0	—	—	1135	0.110	—	—

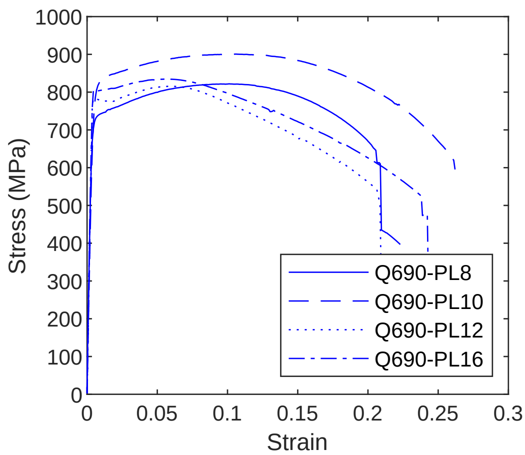

Figure 3. Stress–strain curves of Q690 coupons [21]

2.3 Test setup

The testing was conducted in the Structures Laboratory of South China University of Technology and it utilized a load frame assembly. This assembly, shown in Figure 4, is comprised of interconnected members that form a planar frame. It serves the purpose of transferring forces from a 300t jack and another MTS hydraulic actuator, both of which were installed within the load frame, to the sturdy floor of the laboratory. The T-shaped specimen was positioned within the load frame and secured at the top and bottom of the column using large load pins. These pins were then connected to the crosshead of the jack at the top and to a substantial beam at the bottom of the load frame, which was tied to the strong floor. Such arrangement allowed for unrestricted rotation of the column ends during loading, thereby simulating inflection points at the midpoint of the columns on each story. The load pins were constructed from thick plate material and solid steel dowels. Loading was applied to the top of the column through the jack, and subsequently to the beam tip by the actuator. This actuator, capable of delivering 300 kN of force with a stroke length of ±250 mm, was attached to the beam using a pair of end plates connected by high-strength threaded steel rods. The top of the actuator was firmly fastened to the top beam of the load frame. To prevent any out-of-plane movement of the beam caused by lateral-torsional buckling, a pair of brackets were employed. These brackets were affixed to an additional pair of columns, which were securely fastened to the strong floor. In order to minimize the impact of potential friction between the brackets and the beam, the brackets were designed with rollers.

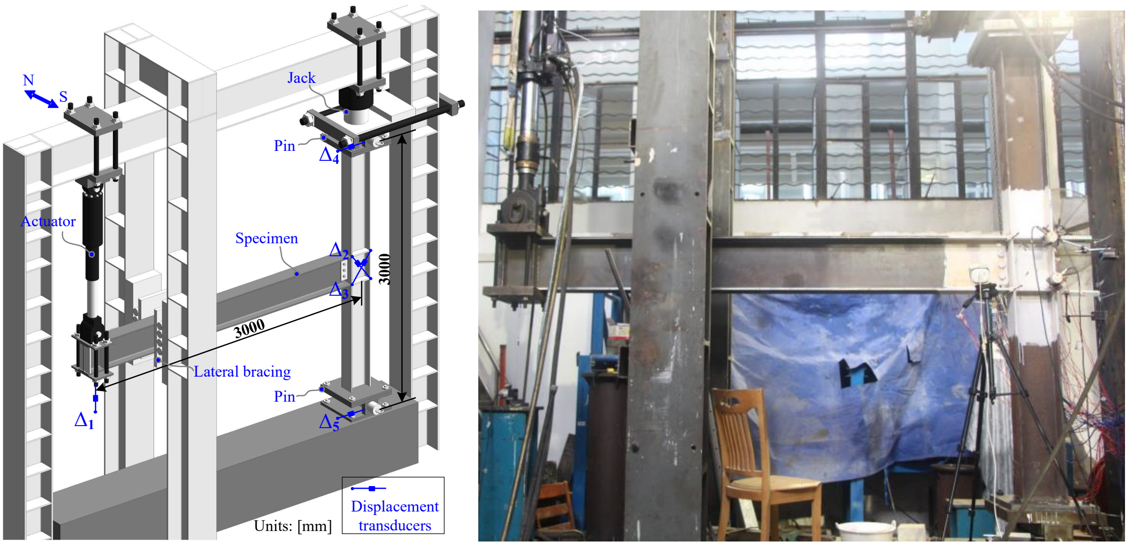

(a) Scheme [21]

(b) On site

Figure 4. Test setup

2.4 Loading protocol

Prior to initiating cyclic loading, an axial compression force was applied to the top of the column to represent seismic weight. This resulted in an axial compression ratio of 0.3 in relation to the nominal axial capacity of the column. This ratio remained consistent across all specimens to maintain uniformity. During the cyclic loading phase, the axial load on the column top remained unchanged. The loading history specified in AISC Seismic Provisions [49] was employed to ensure comparability with numerous other tests conducted during and after the SAC Joint Venture investigations in the United States [48]. This cyclic loading history, based on the story drift angle, deviates from the commonly used approach of employing plastic rotation levels prior to the 1997 Northridge earthquake. The story drift angle is defined as the lateral displacement of the story divided by the height of the story. In this study, the specimens were subjected to displacements at the tip of the beam. Hence, the story drift angle in this context represents the ratio of the displacement at the beam tip to the distance of 3000 mm (equal to $L/2$, where L signifies the column spacing in the prototype frame) between the loading point at the beam tip and the centerline of the column. Figure 5 illustrates the prescribed loading history, with positive story drift angles indicating downward displacements at the beam tip. Since the stroke length of the actuator is ±250 mm, the maximum attainable story drift angle is ±8%. If no significant strength degradation is observed after two cycles at this magnitude, additional cycles at the same amplitude will be conducted until the specimen fails or further substantial strength reduction occurs.

2.5 Instrumentation

To measure the applied load magnitude at the beam tip and column top, load cells were installed on the actuator and the jack, respectively. Figure 4 illustrates the utilization of displacement transducers to isolate the rotation contributions occurring in specific components of each specimen's connection. These components include the shear distortion of the panel zone and

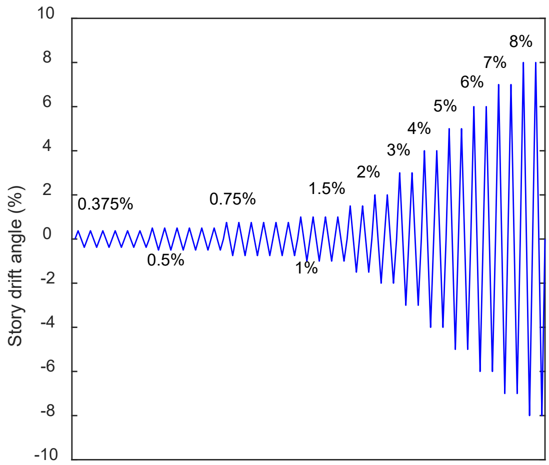

Figure 5. Loading protocol [49]

the plastic hinge rotation in the beam end.

The primary displacement transducer, labeled as DT-1, was employed to measure the displacement at the beam tip and served as the displacement-control signal for the actuator. Diagonally arranged displacement transducers, DT-2 and DT-3, were utilized to measure the average shear deformation of the panel zone. This is particularly significant for specimens designed with a weak panel zone, as the shear distortion of the panel zone contributes significantly to the total story drift angle. Two additional transducers, DT-4 and DT-5, were positioned to monitor the horizontal displacements at the center of pins connected to the top and bottom of the column. Accounting for the possible rigid rotation of the entire specimen, the story drift angle, θ, was calculated by [21]:

$$\theta = \frac{\Delta_1}{L/2} - \frac{\Delta_4 - \Delta_5}{H} \tag{1}$$

where Δ_1, Δ_4 and Δ_5 correspond to the readings from the respective labeled displacement transducers, L is the distance explained earlier as 6000 mm, and H signifies the story height between the pin centerlines, which is 3000 mm. The shear distortion of the panel zone, denoted by γ_{pz}, was calculated by [21]:

$$\gamma_{\mathrm{pz}} = \frac{\Delta_2 - \Delta_3}{2} \frac{\sqrt{b_{\mathrm{pz}}^2 + h_{\mathrm{pz}}^2}}{b_{\mathrm{pz}} h_{\mathrm{pz}}} \tag{2}$$

where Δ_2 and Δ_3 represent readings from the diagonal transducers, b_{pz} and h_{pz} represent the width and height of the panel zone, measured as distances between the column flange centerlines and continuity plate centerlines, respectively. The contribution of the panel zone shear distortion to the displacement at the beam tip, or equivalently, to the story drift angle relative to the column centerline, was determined by [21]:

$$\theta_{\mathrm{pz}} = \left(1 - \frac{h_{\mathrm{b}}}{H}\right) \gamma_{\mathrm{pz}} \tag{3}$$

where h_{b} denotes the beam depth. By subtracting the contribution of the panel zone from the total story drift angle, the rotational contribution of the plastic hinge in the beam end, if present, could be evaluated.

3 Test results

3.1 Failure modes

Failure modes of the specimens are summarized in Figure 6. Although the beam section of H280×160×8×10 is classified as an elastic (or non-compact) section according to Eurocode 3 (Class 3) [54] and Chinese Standard (Class S4) [55], based on its flange slenderness, all specimens eventually fractured before significant local buckling in the beam end. The only specimen welded with backing plates, Specimen B690-C690-PZ16*b*, experienced premature fracture at the bottom CJP groove weld when the story drift angle reached −3.1% in the first negative excursion of 4% (see Figure 6(a)). The loading continued and fracture occurred at the top CJP groove weld when the story drift angle approached 3% in the second positive excursion of this amplitude (see Figure

6(b)). Both fracture phenomena were characterized by the total tear out of the weld metal from the column flange surface. This is a common failure mode for CJP welds with backing plate, since the backing plate hides weld flaws resulting from the weld root pass and provides an initial surface crack depth [48].

In contrast to Specimen B690-C690-PZ16*b*, the three specimens with backing plates removed (i.e., with Type *c* detail) fractured as well but in the beam flange outside the heat affected zone near the weld access hole. Apparently, this kind of fracture in the flange steel allowed for larger deformation than the premature weld fracture mentioned above. To be specific, Specimen B690-C690-PZ16*c*, which had an intermediate panel zone thickness among the three specimens, fractured at the story drift angle of -3.4% of the second cycle of 6% amplitude (see Figure 6(c)). Due to the rapid crack growth across the beam flange, the fracture finished all of a sudden and brought an impact to the web bolts. Hence, the lowest bolt, as shown in Figure 6(c), also fractured in shear. The comparison between Specimens B690-C690-PZ16*c* and B690-C690-PZ16*b* evidenced the effectiveness of removing backing plates to improve connection performance by making the fracture mode more ductile. The specimen with a weaker panel zone, B690-C690-PZ12*c*, survived until the second cycle of 7%, and fracture in the top beam flange occurred when the story drift angle approached 1% in the positive excursion of that cycle (see Figure 6(c)). On the other hand, the specimen of a stronger panel zone with a doubler plate, B690-C690-PZ20*c*, suffered fracture in the beam bottom flange when the story drift angle reached −5.5% at the first negative excursion of 6% (see Figure 6(e)). The panel zone of this specimen was so strong that plastic demand was expected to be concentrated to the beam end. In addition to the fracture observed, slight local buckling was noted in the beam top flange under compression, as shown in Figure 6(e).

3.2 Hysteretic curves

Figure 7 displays the hysteretic curves of all specimens, illustrating the relationship between moment and story drift angle. The moment was calculated as the product of the distance between

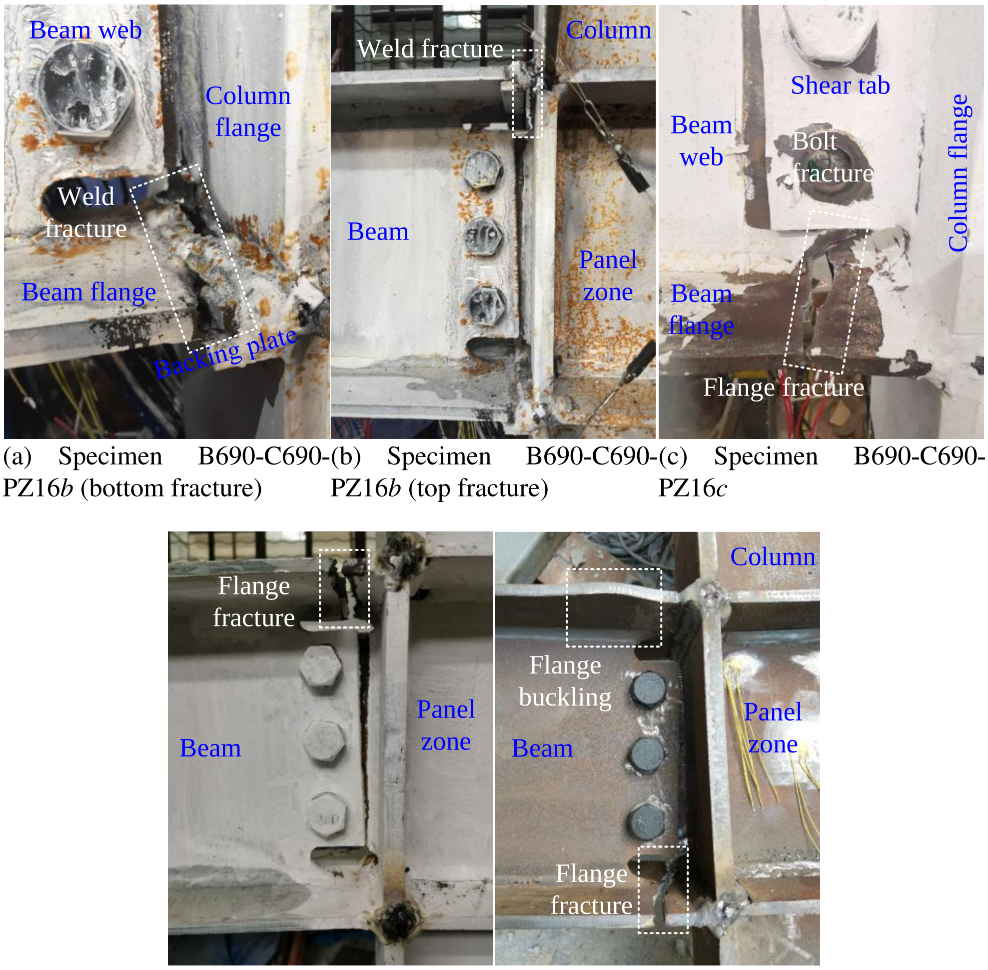

(a) Specimen B690-C690-PZ16*b* (bottom fracture) (b) Specimen B690-C690-PZ16*b* (top fracture) (c) Specimen B690-C690-PZ16*c*

(d) Specimen B690-C690-PZ12*c* (e) Specimen B690-C690-PZ20*c*

Figure 6. Failure modes

the loading point at the beam tip and the column face—specifically, 3000 mm minus half of the column depth—and the reaction force at the beam tip. To provide a basis for comparison, the yielding moment ($M_{y,b}$) and full plastic moment ($M_{p,b}$) of the beam cross section were determined using the measured material properties presented in Table 2 and plotted on the figure.

Furthermore, Figure 8 presents the moment-shear distortion hysteretic curves for the panel zones in all specimens. The moment is that at the column face mentioned earlier, while the shear distortion was determined using Eq. (2). For comparison, the yielding moment of the panel zone ($M_{y,pz}$), taking into account the influence of axial compression and column shear, is indicated in

Figure 8. This yielding moment was calculated using [21]:

$$M_{\mathrm{y,pz}} = \sqrt{1 - \left(\frac{N_{\mathrm{c}}}{f_{\mathrm{yc}} A_{\mathrm{c}}}\right)^2} \frac{f_{\mathrm{yc}}}{\sqrt{3}} b_{\mathrm{pz}} h_{\mathrm{pz}} t_{\mathrm{pz}} \frac{L - h_{\mathrm{c}}}{L} \frac{H}{H - h_{\mathrm{pz}}} \tag{4}$$

where N_{c} represents the axial compression force on the column, $f_{\mathrm{y,c}}$ refers to the material yield strength, h_{c} is the column depth, A_{c} is the cross-sectional area of the column, and t_{pz} corresponds to the thickness of the panel zone. Note that, the ratio $N_{\mathrm{c}}/f_{\mathrm{yc}}A_{\mathrm{c}}$ was maintained as 0.3 in all specimens.

As anticipated, the hysteretic curves exhibited by all specimens were plump without any obvious pinching, stiffness or strength degradation prior to the ultimate fracture, except for Specimen B690-C690-PZ16*b*. Notably, this specific specimen failed due to premature weld fracture. Consequently, inelastic rotation was hardly developed by this specimen, as indicated by the hysteretic response still within the beam yielding moment capacity (Figure 8(a)). The specimens with intermediate and strong panel zones as well as Type *c* backing plate detail, B690-C690-PZ16*c* and B690-C690-PZ20*c*, exhibited yielding moment capacity of the beam but did not attain its full plastic capacity (Figure 8(b) and 8(d)). This is also under expectation because of the non-compact beam section used in this study. However, in Specimen B690-C690-PZ12*c*, because of the weak panel zone, the ultimate moment could not reach the beam yielding capacity (Figure 8(c)). The panel zone of this specimen yielded before the beam.

With regard to the responses of the panel zones, the specimen with the weakest panel zone, B690-C690-PZ12*c*, developed a plump and full hysteretic curve. Notable agreement with the yielding moment predicted by Eq. (4) was observed in this specimen, as depicted in Figure 8(c). It is intriguing to observe that the Q690 high-strength steel panel zone demonstrated remarkable inelastic shear distortions, as evidenced by this specimen. Noteworthy plastic hardening was additionally observed within this panel zone, attributable to the strain hardening of the material and the involvement of the column flanges in shear transfer subsequent to the initial onset of

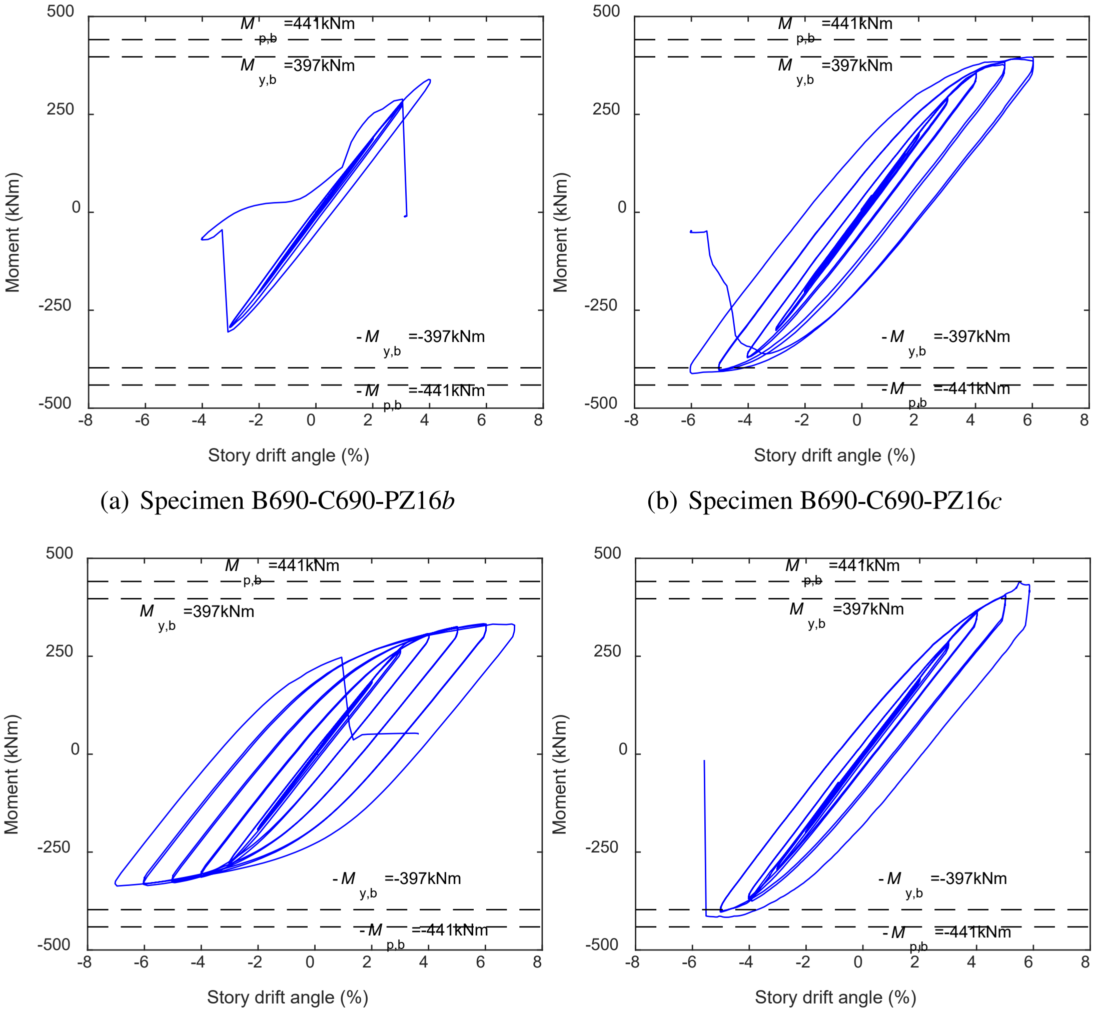

(a) Specimen B690-C690-PZ16*b*

(b) Specimen B690-C690-PZ16*c*

(c) Specimen B690-C690-PZ12*c*

(d) Specimen B690-C690-PZ20*c*

Figure 7. Moment–story drift angle hysteretic curves

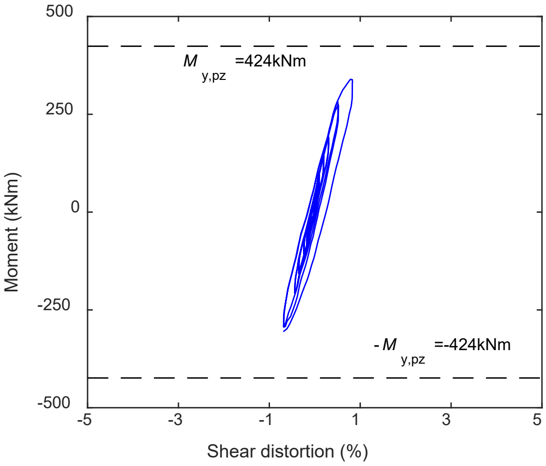

(a) Specimen B690-C690-PZ16*b*

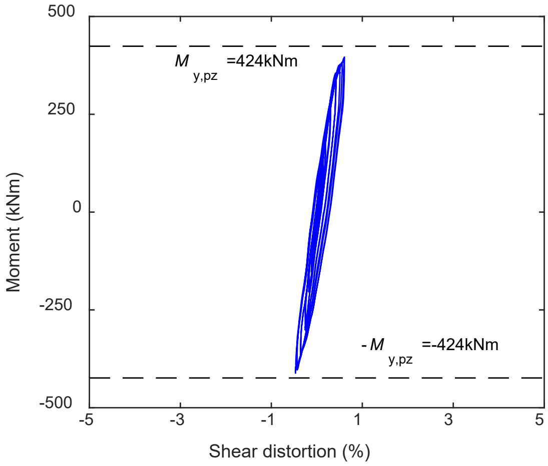

(b) Specimen B690-C690-PZ16*c*

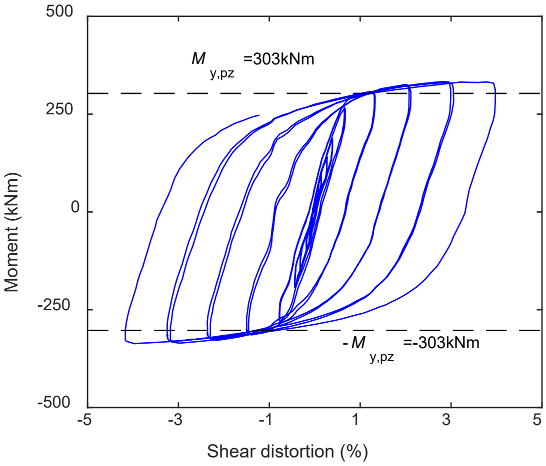

(c) Specimen B690-C690-PZ12*c*

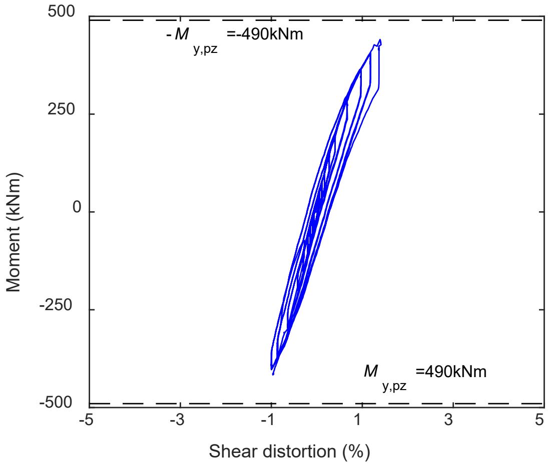

(d) Specimen B690-C690-PZ20*c*

Figure 8. Moment–shear distortion hysteretic curves

yielding in the web panel. This particular test provides experimental support for the reliability of energy dissipation through panel zone yielding, even when employing 690 MPa high-strength steel. It should be noted that the maximum inelastic shear distortion that was achieved by Specimen B690-C690-PZ12*c* is about 0.03 rad, but this is not the real deformation capacity of the panel zone since no shear failure was observed. In fact, the previous testing on dual-steel connections showed that the 690 MPa steel panel zone could sustain as large a plastic shear distortion as nearly 0.04 rad [21]. The other specimens with intermediate or strong panel zones exhibited basically elastic responses in their panel zones.

3.3 Strength, deformation and energy dissipation capacities

The determination of the elastic stiffness, denoted as K_e, was based on the hysteretic curves represented in Figure 7. Linear regression was employed to fit the data within a 2% amplitude range, and the resulting values are presented in Table 3. It is important to highlight that K_e represents the stiffness of the entire beam-to-column assembly, rather than the rotational stiffness of the connection itself. The ultimate (or maximum) moment, denoted as M_u, was determined by averaging maximum positive and negative moments and is also summarized in Table 3. Specimens featuring panel zones with thicknesses of 16 mm or 20 mm demonstrated robust panel zone design, as their $M_{y,pz}$ values surpassed the M_u values. In contrast, the specimen with a 12-mm-thick panel zone, B690-C690-PZ12*c*, exhibited a lower $M_{y,pz}$ value compared to $M_{y,b}$, indicating that its performance was primarily influenced by the panel zone. The level of overstrength, defined as the ratio of the ultimate moment M_u to the yield moment M_y (the minimum between $M_{y,b}$ and $M_{y,pz}$), is included in Table 3. With the exception of the specimen featuring Type *b* connection detail (B690-C690-PZ16*b*), which experienced premature fracture, the other specimens with Type *c* detail demonstrated maximum moments (M_u) exceeding the yield moment (M_y), although this overstrength remained within 10%. This suggests that some degree of inelastic rotation should be anticipated at the beam end or in the panel zone. The specimen with the weakest panel zone (B690-C690-PZ12*c*) exhibited moderate strain hardening, as indicated by its M_u/M_y (or $M_u/M_{y,pz}$) ratio of 1.1, slightly higher than that of the other specimens with stronger panel zones (B690-C690-PZ16*c* and B690-C690-PZ20*c*). It is important to note that the ultimate moments (M_u) observed in all specimens were below the full plastic moments of the beam ($M_{p,b}$), due to the utilization of non-compact beam sections in these specimens.

Table 3. Stiffness and strength

Specimen label	K_e (kNm)	$M_{p,b}$ (kNm)	$M_{y,b}$ (kNm)	$M_{y,pz}$ (kNm)	M_y (kNm)	M_u (kNm)	$\frac{M_u}{M_y}$	$\frac{M_u}{M_{p,b}}$
B690-C690-PZ16*b*	9933	441	397	424	397	323	0.81	0.73
B690-C690-PZ16*c*	9987					404	1.02	0.92
B690-C690-PZ12*c*	9469			303	303	335	1.10	0.76
B690-C690-PZ20*c*	9442			490	397	429	1.08	0.97

Table 4 provides a summary of various parameters pertaining to deformation and energy dissipation capacities. The yield story drift angle, denoted as θ_y, was determined by calculating the ratio of the yield moment, M_y, to the elastic stiffness, K_e. The ultimate story drift angle, θ_u, was considered valid only if at least one complete cycle of the target story drift angle was achieved prior to fracture [48]. The plastic story drift angle, θ_p, which represents the plastic rotation relative to the column centerline, was determined as the plastic component of θ_u. Additionally, Table 4 presents the plastic rotation component in the beam, $\theta_{p,b}$, as well as in the panel zone, $\theta_{p,pz}$. The plastic rotation of the panel zone, $\theta_{p,pz}$, was deduced from the total rotation of the panel zone, θ_{pz}, defined in Eq. (3). On the other hand, the plastic rotation of the beam, $\theta_{p,b}$, was obtained by subtracting $\theta_{p,pz}$ from θ_p. Consequently, the ductility factor, μ, was computed as the ratio of θ_u to θ_y. Furthermore, cumulative plastic rotations, $\Sigma\Delta\theta_p$, and energy dissipation, ΣA, for the entire set of specimens were evaluated using the approach described in ATC-24 [56, 57] and depicted in Figure 9. It should be noted that these quantities were considered up until the last successful excursion (or half-cycle) prior to fracture, and their normalized values were also included in Table 4, denoted as $\Sigma\Delta\theta_p/\theta_y$ and $\Sigma A/\left(M_y\theta_y\right)$, respectively.

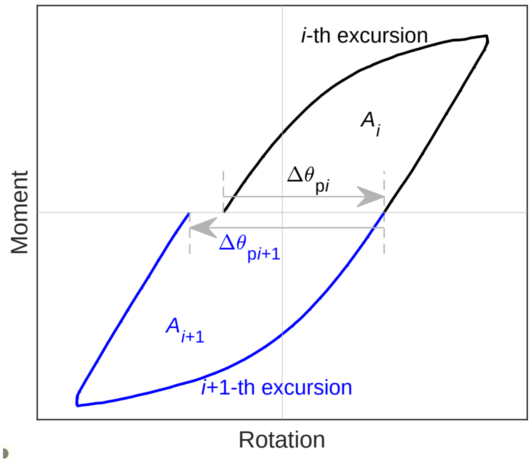

Figure 9. Definition of cumulative plastic rotation and energy dissipation in ATC-24 [56]

Table 4. Deformation and energy dissipation

Specimen label	θ_y (rad)	θ_u (rad)	μ	θ_p (rad)	$\theta_{p,pz}$ (rad)	$\theta_{p,b}$ (rad)	$\Sigma\Delta\theta_p$	$\frac{\Sigma\Delta\theta_p}{\theta_y}$	ΣA (kJ)	$\frac{\Sigma A}{M_{y,min}\theta_y}$
B690-C690-PZ16*b*	0.040	0.03	0.8	0.002	0.001	0.001	0.028	0.7	6.0	0.4
B690-C690-PZ16*c*	0.040	0.06	1.5	0.021	0.002	0.019	0.252	6.3	86.6	5.3
B690-C690-PZ12*c*	0.032	0.07	2.2	0.035	0.030	0.005	0.515	16.1	146.1	14.5
B690-C690-PZ20*c*	0.042	0.05	1.2	0.010	0.002	0.008	0.142	3.4	49.1	2.8

It is evident that, with the exception of Specimen B690-C690-PZ16*b*, all specimens displayed substantial story drift angles and achieved satisfactory performance, considering a story drift angle of 0.04 rad as an acceptable criterion for Special Moment Frames (SMF) according to AISC Seismic Provisions [49]. However, due to the utilization of high-strength steel materials and relatively small beam and column sections in this study, the yield drift angles of these specimens reached nearly 0.04 rad, approximately four times the traditionally expected yield drift angle (around 0.01 rad) for moment connections made of conventional-strength steel. Consequently, if a plastic rotation of 0.03 rad is deemed necessary for SMF, only the specimen featuring the weakest panel zone and Type *c* detail (B690-C690-PZ12*c*) is considered to possess sufficient rotation capacity. The other two specimens with stronger panel zones and Type *c* detail (B690-C690-PZ16*c* and B690-C690-PZ20*c*) demonstrated plastic rotations ranging from 0.01 to

0.02 rad, which are only suitable for Intermediate Moment Frames (IMF) [49].

Remarkably, when comparing the three specimens with Type *c* detail but varying panel zone thicknesses, it is apparent that the weak panel zone contributes to an increased overall plastic rotation capacity. This is noteworthy because it has conventionally been believed that excessive deformation in the panel zone adversely affects rotation capacity due to the formation of a "kink" in the column flanges, leading to significant local stress or strain concentrations near the flange welds. However, this adverse effect was not observed in the present study. The Q690-grade panel zone in this study sustained a plastic shear rotation as large as approximately 0.03 rad, and there was no failure in the panel zone even at this magnitude, as demonstrated by Specimen B690-C690-PZ12*c*. This shear rotation quantity aligns with a previous test conducted by the authors [21], which revealed an ultimate plastic rotation capacity of around 0.04 rad for a Q690 panel zone of similar size to the one investigated in this study.

Additionally, the cumulative quantities indicate a more ductile behavior in the panel zone compared to the beam end. In the case of plastic shear in the panel zone, the cumulative plastic rotation is 16 times greater than the yield rotation, whereas for plastic bending in the beam end, it is only 3 to 6 times larger. A similar comparison can be made regarding the cumulative energy dissipation. Normalizing the cumulative plastic rotation based on the maximum plastic rotation, the normalized values range from 12 to 15 for the three specimens with Type *c* weld detail. These seismic capacities exceed the conventionally anticipated seismic demand, which suggests that the cumulative plastic deformation should be 5 to 8 times larger than the maximum plastic deformation [57, 58].

4 Discussion

4.1 CJP groove weld details

In current Chinese seismic design codes pertaining to steel structures [45, 47, 55], the welding detail denoted as Type *b* in this paper is prescribed for connection of beam and column flanges by means of CJP welds. In contrast, the United States imposes more stringent weld detail requirements for ductile moment frames. For instance, AISC Prequalified Connections [51] for SMF or IMF recommend a welded flange-welded web connection. In this connection, a CJP weld with backing plate that is reinforced by a fillet weld is executed at the upper beam-to-column flange connection, while a CJP weld without a backing plate or one that is removed after the welding process is specified for the lower connection.

Nonetheless, the findings of the current investigation demonstrate that Type *b* weld detail fails to ensure ductile performance, as evidenced by premature fracture observed in Specimen B690-C690-PZ16*b* at their CJP welds. Moreover, it is worth noting that even the AISC-prescribed weld details for welded flange-welded web connections may prove insufficient, given that the CJP weld with a backing plate, although reinforced by a fillet weld at the bottom beam flange, still experienced fracture in the above specimen. In contrast, the specimens employing Type *c* detail exhibited relatively ductile behavior, characterized by fracture occurring in the beam flange.

In fact, a prior study conducted by the authors [21] had previously affirmed the reliability of employing Type *b* weld detail in dual-steel connections, specifically for connecting conventional-strength steel beam flanges to a high-strength steel column. This disparity in performance is likely attributable to the diminished material ductility inherent in Q690 high-strength steel when compared to its conventional-strength counterparts. Consequently, it is concluded that in the case of Q690 high-strength steel welded flange-bolted web connections, the CJP welds should be executed by removing backing plates, performing backgouging, and further reinforcing the weld root by a fillet weld. While this weld detail, denoted as Type *c* in this study, is considerably costlier than Type *b*, its adoption is imperative to avert the risk of brittle fracture in high-strength steel connections, as elucidated in this research.

In the context of continuity plate welds, this study has provided noteworthy insights. Current Chinese design codes and AISC Seismic Provisions commonly stipulate the use of CJP groove welds in the connection between continuity plates and column flanges. However, they permit the utilization of fillet welds between continuity plates and the column web. In this investigation, an unintentional use of fillet welds was in all specimens for continuity plate-to-column flange connections. Interestingly, these fillet welds demonstrated commendable performance, provided they were of sufficient size. This observation, along with the previous test results by the authors [21], underscores the advantage of employing cost-effective fillet welds rather than more expensive CJP groove welds even in case of high-strength steel, a benefit that has also been substantiated in conventional-strength steel welded flange-welded web connections [59, 60].

4.2 Balanced design between the beam and panel zone

A major focus in this study is to evaluate the effect of panel zone strength on connection performance. Hence, the existing panel zone design methodologies were compared. Capacity-to-demand ratios for the panel zones in all specimens have been consolidated and presented in Table 5. These ratios elucidate the degree to which the panel zones can withstand the specified demand levels, as stipulated in the design codes originating from China, the United States, and Europe, in accordance with the following expressions [21]:

$$\frac{4}{3}\frac{f_{\mathrm{y,pz}}}{\sqrt{3}}h_{\mathrm{pz}}b_{\mathrm{pz}}t_{\mathrm{pz}} \geq \alpha_{\mathrm{pz}}\Sigma W_{\mathrm{y,b}}f_{\mathrm{y,b}} \tag{5}$$

$$0.6f_{\mathrm{y,pz}}\frac{0.95h_{\mathrm{c}}t_{\mathrm{pz}}h_{\mathrm{b}}}{\beta}\left(1+\frac{3b_{\mathrm{c}}t_{\mathrm{fc}}^{2}}{h_{\mathrm{b}}h_{\mathrm{c}}t_{\mathrm{pz}}}\right) \geq \min\left(\frac{f_{\mathrm{y,b}}+f_{\mathrm{u,b}}}{2f_{\mathrm{y,b}}}, 1.2\right)\Sigma W_{\mathrm{y,b}}f_{\mathrm{y,b}} \tag{6}$$

$$(0.9)\,0.55f_{\mathrm{y,pz}}h_{\mathrm{c}}t_{\mathrm{pz}} \geq \frac{\Sigma W_{\mathrm{y,b}}f_{\mathrm{y,b}}}{h_{\mathrm{b}}}\left(\frac{L}{L-h_{\mathrm{c}}}\right)\left(\frac{H-h_{\mathrm{b}}}{H}\right) \tag{7a}$$

$$(0.6)\,0.55f_{\mathrm{y,pz}}h_{\mathrm{c}}t_{\mathrm{pz}} \leq \frac{\Sigma W_{\mathrm{y,b}}f_{\mathrm{y,b}}}{h_{\mathrm{b}}}\left(\frac{L}{L-h_{\mathrm{c}}}\right)\left(\frac{H-h_{\mathrm{b}}}{H}\right) \tag{7b}$$

$$0.9\frac{f_{y,pz}}{\sqrt{3}}\frac{(h_c-2t_{fc})\,h_{pz}t_{pz}}{\beta}+\frac{2M_{p,fc}+\min\left(2M_{p,fc},2M_{p,st}\right)}{\beta}\geq\Sigma W_{y,b}f_{y,b} \tag{8}$$

Eq. (5) is from Chinese Standard [55], Eq. (6) is from AISC Seismic Provisions [49], Eqs. (7) denote lower and upper bounds for the panel zone resistance suggested by FEMA [48], and Eq. (8) is from Eurocode 8 [61]. In the above equations, $f_{y,pz}$ is the yield strength of the panel zone material; $f_{y,b}$ and $f_{u,b}$ are yield and tensile strength of the beam material, respectively; $W_{y,b}$ is the elastic section modulus of the beam; b_c and t_{fc} are the width and thickness of the column flange, respectively; $M_{p,fc} = b_c t_{fc}^2 f_{y,cf}/4$ and $M_{p,st} = b_c t_{st}^2 f_{y,st}/4$ are plastic moment resistances of the column flange and a pair of continuity plates, respectively, where t_{st} and $f_{y,st}$ are the thickness and material yield strength of the continuity plates, respectively; α_{pz} is a coefficient taken as 0.95 for one-sided connections; β is another coefficient called transformation parameter to account for the effect of column shears and it should be determined based on the internal force equilibrium. Note that, as the beam sections are non-compact in this study, the elastic section modulus ($W_{y,b}$) rather than the plastic one ($W_{p,b}$) is used to estimate the beam strength.

Evidently, the panel zones exhibit a varying degree of capacity depending on the design code employed, with the weakest panel zone, characterized by the largest capacity-to-demand ratio, emerging under Chinese Standard design practices. Conversely, the most robust panel zone, denoted by the smallest ratio, is observed when adhering to Eurocode 8, as has been corroborated in earlier investigations [21, 35]. It is noteworthy that the panel strength prescribed by Eurocode 8 aligns closely with the bounds defined by FEMA. In contrast, the panel strength requirements stipulated by Chinese and AISC codes fall below the lower FEMA bound.

All specimens met the panel zone strength criteria outlined in Chinese Standard, as evidenced by their capacity-to-demand ratios exceeding 1. Similarly, compliance with AISC Seismic Provisions was also achieved across all specimens. However, only Specimen B690-C690-PZ12*c* failed to meet the panel strength criterion in Eurocode 8, as indicated by its ratio less than 1.

Interestingly, this particular specimen exhibited superior plastic rotation and energy dissipation capacities. These findings suggest that the criterion in Eurocode 8 for minimum panel zone strength may warrant reconsideration and relaxation in high-strength steel connections, since the advantageous role played by high-strength steel panel zones in dissipating energy is affirmed through a direct comparison of their plastic rotation capacity (exceeding 0.03 rad) with that of the beam end (ranging from 0.01 to 0.02 rad), as documented in Table 4.

Table 5. Capacity-to-demand ratios of panel zones

Specimen label	Chinese Standard	AISC Seismic Provisions	FEMA		Eurocode 8
			Lower bound	Upper bound	
B690-C690-PZ12*c*	1.04	1.00	0.76	0.51	0.75
B690-C690-PZ16*b* B690-C690-PZ16*c*	1.46	1.34	1.06	0.71	1.02
B690-C690-PZ20*c*	1.69	1.52	1.23	0.82	1.17

5 Conclusions

This paper reports on an experimental investigation into the cyclic response of Q690-grade high-strength steel beam-to-column connections, specifically focusing on welded flange-bolted web connections. A set of four one-sided connection specimens was tested, with the primary objective of assessing the impact of beam-to-column flange weld details and panel zone strength. The study yields the following conclusions:

1) The connection using backing plates and reinforced with a fillet weld underneath the bottom beam flange, exhibited brittle fracture at CJP welds without development of any plastic rotation. The other connections with all backing plates removed and CJP weld roots backgouged and further reinforced by fillet welds, exhibited ductile fracture at beam flanges. Hence, the weld detail not using backing plates or removing them after the welding process is strongly recommended for 690 MPa high-strength steel welded flange-bolted web connections.

2) The strong-panel-zone connections without backing plates developed very slight strain hardening, and their maximum moment resistances were very close to the beam yielding moment. These connections sustained plastic rotations of 0.01–0.02 rad in the beam end, and cumulative plastic rotations of about 3–6 times larger than the yielding rotation.
3) The weak-panel-zone connection without backing plates exhibited slight strain hardening by developing a 10% larger maximum moment resistance than the yielding moment of the panel zone. This connection achieved a plastic rotation of 0.03 rad in the panel zone, and a cumulative plastic rotation of about 16 times larger than the yielding rotation, until fracture in the beam end. Yielding of the panel zone did not show adverse effect on the total plastic rotation capacity of the connection.

It should be noted that, in this experimental study, the connections made with relatively shallow beams (280 mm in depth) were evaluated. Further study on high-strength steel moment connections with larger size beams, especially those with deeper beam sections, is needed.

Acknowledgments

The authors would like to acknowledge the financial supports for this work by the National Natural Science Foundation of China (Grant Nos. 51638009, 51978279 and 52108145), Guangdong Basic and Applied Basic Research Foundation (Grant Nos. 2021A1515010610 and 2023A1515010047) and Fundamental Research Funds for the Central Universities (Grant No. 2023ZYGXZR098).

References

[1] J. Raoul, H.-P. Günther, Use and application of high-performance steels for steel structures, International Association for Bridge and Structural Engineering (IABSE), Zürich, Switzerland, 2005.

[2] Y. Fukumoto, New constructional steels and structural stability, Engineering Structures 18 (1996) 786–791.

[3] R. Bjorhovde, Development and use of high performance steel, Journal of Constructional Steel Research 60 (2004) 393–400.

[4] G. Shi, F. Hu, Y. Shi, Recent research advances of high strength steel structures and codification of design specification in China, International Journal of Steel Structures 14 (2014) 873–887.

[5] G. Shi, X. Chen, Research advances in HSS structures at Tsinghua University and codification of the design specification, Steel Construction 11 (2018) 286–293.

[6] H. Ban, G. Shi, A review of research on high-strength steel structures, Proceedings of the Institution of Civil Engineers - Structures and Buildings 171 (2018) 625–641.

[7] D. Dubina, A. Stratan, F. Dinu, Re-centring capacity of dual-steel frames, Steel Construction 4 (2011) 73–84.

[8] D. Dubina, F. Dinu, A. Stratan, High-strength steel and dissipative fuse solutions for seismic-resistant building structures, Steel Construction 13 (2020) 154–164.

[9] D. Dubina, F. Dinu, A. Stratan, Resilience of dual steel-dual frame buildings in seismic areas, Steel Construction 14 (2021) 150–166.

[10] H. Ban, G. Shi, Y. Shi, Y. Wang, Research progress on the mechanical property of high strength structural steels, Advanced Materials Research 250-253 (2011) 640–648.

[11] G. Shi, X. Zhu, H. Ban, Material properties and partial factors for resistance of high-strength steels in China, Journal of Constructional Steel Research 121 (2016) 65–79.

[12] F. Hu, G. Shi, Constitutive model for full-range cyclic behavior of high strength steels without yield plateau, Construction and Building Materials 162 (2018) 596–607.

[13] H. Kuwamura, T. Suzuki, Low-cycle fatigue resistance of welded joints of high-strength steel under earthquake loading, in: A. L. Arroyo, R. Blázquez, J. Martí (Eds.), Proceedings of the Tenth World Conference on Earthquake Engineering, Balkema, Rotterdam, Madrid, Spain, 1992, pp. 2851–2856.

[14] D. Dubina, A. Stratan, N. Muntean, F. Dinu, Experimental program for evaluation of moment beam-to-column joints of high strength steel components, in: R. Bjorhovde, F. S. K. Bijlaard, L. F. Geschwindner (Eds.), Proceedings of the Sixth International Workshop on Connections in Steel Structures VI, American Institute of Steel Construction, Chicago, Illinois, USA, 2008, pp. 355–366.

[15] S.-H. Oh, H.-Y. Park, A study to enhance the deformation capacity of beam-to-column connections using high strength steel having high yield ratio, International Journal of Steel Structures 16 (2016) 73–89.

[16] F. Liao, X. Li, W. Wang, Y. Chen, T. Zhou, S. Nie, G. Li, Seismic performance study on Q460 high-strength steel welded cruciform beam-column connections, Journal of Constructional Steel Research 198 (2022) 107504.

[17] X. Liu, Y. Wang, Y. Shi, Q. Tan, Experimental study on low-cycle fatigue fracture behavior of high strength steel beam-to-column connection, Journal of Building Structures 39 (2018) 28–36. (in Chinese).

[18] J. Lu, Experimental research on the seismic performance of beam-to-column connections in high strength steel

frame, 2015. (in Chinese).

[19] S. Nie, J. Li, H. Wang, Y. Deng, Z. Chen, M. Elchalakani, M. Liu, Seismic behavior of welded high-performance steel beam-to-column joints with different reinforced configurations, Journal of Constructional Steel Research 210 (2023) 108113.

[20] X. Qiang, Y. Shu, X. Jiang, Experimental and numerical study on high-strength steel flange-welded web-bolted connections under fire conditions, Journal of Constructional Steel Research 192 (2022) 107255.

[21] F. Hu, Z. Wang, Cyclic behavior of dual-steel beam-to-column welded flange-bolted web connections, Thin-Walled Structures (2023) 111452. doi:https://doi.org/10.1016/j.tws.2023.111452.

[22] A. M. Girão Coelho, F. S. K. Bijlaard, Experimental behaviour of high strength steel end-plate connections, Journal of Constructional Steel Research 63 (2007) 1228–1240.

[23] X. Lin, T. Okazaki, M. Nakashima, Bolted beam-to-column connections for built-up columns constructed of h-sa700 steel, Journal of Constructional Steel Research 101 (2014) 469–481.

[24] F. F. Sun, X. Y. Xue, H. J. Jin, M. Sun, Z. M. Tang, Y. Xiao, G. Q. Li, Hysteretic behavior and simplified simulation method of high-strength steel end-plate connections under cyclic loading, Journal of Constructional Steel Research 158 (2019) 429–442.

[25] G. Liang, Z. Lu, H. Guo, Y. Liu, D. Yang, S. Li, X. Pan, Experimental and numerical investigation on seismic performance of extended stiffened end-plate joints with reduced beam section using high strength steel, Thin-Walled Structures 169 (2021) 108434.

[26] T. Lin, Z. Wang, F. Hu, P. Wang, Finite-element analysis of high-strength steel extended end-plate connections under cyclic loading, Materials 15 (2022) 2912.

[27] A. Ataei, M. A. Bradford, H. R. Valipour, X. Liu, Experimental study of sustainable high strength steel flush end plate beam-to-column composite joints with deconstructable bolted shear connectors, Engineering Structures 123 (2016) 124–140.

[28] X. Qiang, F. S. Bijlaard, H. Kolstein, X. Jiang, Behaviour of beam-to-column high strength steel endplate connections under fire conditions – Part 1: Experimental study, Engineering Structures 64 (2014) 23–38.

[29] X. Qiang, X. Jiang, F. S. Bijlaard, H. Kolstein, Y. Luo, Post-fire behaviour of high strength steel endplate connections — Part 1: Experimental study, Journal of Constructional Steel Research 108 (2015) 82–93.

[30] X. Qiang, N. Wu, X. Jiang, Y. Luo, F. Bijlaard, Experimental and numerical analysis on full high strength steel extended endplate connections in fire, International Journal of Steel Structures 18 (2018) 1350–1362.

[31] X. Qiang, N. Wu, Y. Luo, X. Jiang, F. Bijlaard, Experimental and theoretical study on high strength steel extended endplate connections after fire, International Journal of Steel Structures 18 (2018) 609–634.

[32] Z. Chen, W. Wang, Z. Wang, Experimental study on high-strength q460 steel extended end-plate connections at elevated temperatures, Journal of Constructional Steel Research 200 (2023) 107686.

[33] P. Lu, J. Yang, T. Ran, W. Wang, Experimental study on flexural capacity and fire resistance of high strength q690 steel flush end-plate connections, Thin-Walled Structures 184 (2023) 110506.

[34] F. Hu, G. Shi, Y. Shi, Experimental study on seismic behavior of high strength steel frames: Global response, Engineering Structures 131 (2017) 163–179.

[35] F. Hu, G. Shi, Experimental study on seismic behavior of high strength steel frames: Local response, Engineering Structures 229 (2021) 111620.

[36] X. Chen, G. Shi, Experimental study on seismic behaviour of cover-plate joints in high strength steel frames, Engineering Structures 191 (2019) 292–310.

[37] X. Chen, G. Shi, Cyclic tests on high strength steel flange-plate beam-to-column joints, Engineering Structures 186 (2019) 564–581.

[38] H. Guo, X. Zhou, W. Li, Y. Liu, D. Yang, Experimental and numerical study on seismic performance of Q690 high-strength steel plate reinforced joints, Thin-Walled Structures 161 (2021) 107510.

[39] S. Jiang, G. Shi, N. Zhang, H. Zhao, T. Sun, Experimental study on seismic behavior of cover-plate connections between steel beams and high strength steel box columns, Thin-Walled Structures 193 (2023) 111208.

[40] S. Jiang, G. Shi, N. Zhang, L. Hou, H. Zhao, Experimental study on seismic behavior of high strength steel flange-plate connections with box columns, Thin-Walled Structures 194, Part A (2024) 111285.

[41] Q. Yang, H. Ban, Balanced design philosophy of superior high-performance steel cover-plated beam-to-column joints, Thin-Walled Structures 184 (2023) 110470.

[42] A. M. Girão Coelho, F. S. K. Bijlaard, H. Kolstein, Experimental behaviour of high-strength steel web shear panels, Engineering Structures 31 (2009) 1543–1555.

[43] S. Jordão, L. Simões da Silva, R. Simões, Design formulation analysis for high strength steel welded beam-to-column joints, Engineering Structures 70 (2014) 63–81.

[44] P. Luo, T. Tanaka, H. Asada, Experimental study on elastic-plastic behavior of high-strength steel beam-to-column panel zone considering under-matching welding effect, Engineering Structures 267 (2022) 114655.

[45] Ministry of Housing and Urban-Rural Development of the People's Republic of China (MOHURD), Technical specification for steel structure of tall building. JGJ 99-2015, China Building Industry Press, Beijing, China, 2015. (in Chinese).

[46] SAC Joint Venture, Recommended Seismic Design Criteria for New Steel Moment-Frame Buildings, FEMA-350, Federal Emergency Management Agency, Washington, D.C., USA, 2000.

[47] Ministry of Housing and Urban-Rural Development of the People's Republic of China (MOHURD), Code for seismic design of buildings (2016 edition). GB 50011-2010, China Building Industry Press, Beijing, China, 2016. (in Chinese).

[48] SAC Joint Venture, State of the Art Report on Connection Performance, FEMA-355D, Federal Emergency Management Agency, Washington, D.C., USA, 2000.

[49] American Institute of Steel Construction (AISC), Seismic Provisions for Structural Steel Buildings. ANSI/AISC 341-22, American Institute of Steel Construction, Chicago, Illinois, USA, 2022.

[50] Ministry of Housing and Urban-Rural Development of the People's Republic of China (MOHURD), Technical specification for high strength bolt connections of steel structures. JGJ 82-2011, China Building Industry Press, Beijing, China, 2011. (in Chinese).

[51] American Institute of Steel Construction (AISC), Prequalified Connections for Special and Intermediate Steel Moment Frames for Seismic Applications. ANSI/AISC 358-22, American Institute of Steel Construction, Chicago, Illinois, USA, 2022.

[52] Ministry of Housing and Urban-Rural Development of the People's Republic of China (MOHURD), Standard for design of high strength steel structures. JGJ/T 483-2020, China Building Industry Press, Beijing, China, 2020. (in Chinese).

[53] Standardization Administration of China (SAC), Metallic materials–Tensile testing–Part 1: Method of test at room temperature. GB/T 228.1-2021, Standards Press of China, Beijing, China, 2021. (in Chinese).

[54] European Committee for Standardization (CEN), Eurocode 3: Design of steel structures - Part 1-1: General rules and rules for buildings. EN 1993-1-1:2005, British Standards Institution (BSI), London, UK, 2005.

[55] Ministry of Housing and Urban-Rural Development of the People's Republic of China (MOHURD), Standard for design of steel structures. GB 50017-2017, China Building Industry Press, Beijing, China, 2017. (in Chinese).

[56] Applied Technology Council (ATC), Guidelines for cyclic seismic testing of components of steel structures. ATC-24, Applied Technology Council, Redwood City, California, USA, 1992.

[57] M. Nakashima, K. Suita, K. Morisako, Y. Maruoka, Tests of welded beam-column subassemblies. I: Global behavior, ASCE Journal of Structural Engineering 124 (1998) 1236–1244.

[58] M. Nakashima, K. Saburi, B. Tsuji, Energy input and dissipation behaviour of structures with hysteretic dampers, Earthquake Engineering and Structural Dynamics 25 (1996) 483–496.

[59] D. Lee, S. C. Cotton, J. F. Hajjar, R. J. Dexter, Y. Ye, Cyclic behavior of steel moment-resisting connections reinforced by alternative column stiffener details. I: Connection performance and continuity plate detailing, AISC Engineering Journal 42 (2005) 189–213.

[60] M. Reynolds, C.-M. Uang, Economical weld details and design for continuity and doubler plates in steel special moment frames, ASCE Journal of Structural Engineering 148 (2022) 04021246.

[61] European Committee for Standardization (CEN), Eurocode 8: Design of structures for earthquake resistance - Part 1: General rules, seismic actions and rules for buildings. EN 1998-1:2004, British Standards Institution (BSI), London, UK, 2004.